Kinematic Design and Analysis for a Macaque Upper-Limb Exoskeleton with Shoulder Joint Alignment

Kevin Haninger, Junkai Lu, Wenjie Chen and Masayoshi Tomizuka

***Abstract*— An exoskeleton design for a rhesus macaque subject is motivated, presented, and analyzed. As kinematic properties of the macaque's upper-limb have not been thoroughly studied, this paper introduces methods to determine properties relevant to exoskeleton design. Alignment with biological joints is critical for exoskeleton performance, but there are no accepted kinematic joint models for rhesus macaques. An algorithm is introduced which uses motion capture data to determine an appropriate model for the shoulder complex. An exoskeleton which incorporates this model is introduced, then analyzed. As joint speeds of macaques are also not well studied, a proposed analysis finds an upper bound on the joint speeds required to realize a given end effector speed in an arbitrary direction for all configurations within the workspace.**

I. INTRODUCTION

Exoskeletons are a class of mechanical systems which, when attached to a subject at key locations, allow force-displacement interactions between the mechanism and the subject. Pressures at contact points induce joint torques on the subject, while the displacements of the contact points allow the exoskeleton to infer the subject's joint angles. These interactions form the basis of exoskeleton applications which range from rehabilitation to power augmentation. Here, the exoskeleton is being developed for a brain-machine interface, where real-time neural activity of the subject is measured, and the intended motion of the subject inferred by a decoder. The estimated desired motion is then realized by an upper-limb exoskeleton, which uses torque, position, or impedence control in a reaching task, as seen in Fig. 1.

Due to the invasive nature of the neural measurements, the subjects of this study are *Macaca mulattas*, or rhesus macaques. As the macaque morphology bears similarities to humans, results from the field of upper-limb exoskeleton design for humans can serve as reference, but care must be taken on extending models based on the physiology of humans to macaque subjects. Critical to machine-subject interaction is the safety of the subject, here made difficult by the novelty of macaque exoskeletons and the lack of explicit communication with the subject. Additionally, as discomfort of the subject may interfere with the neural motor control which is being studied, the emphasis of this work is on an ergonomic design. This goal is pursued by improving alignment of the exoskeleton joints with the biological joints, particularly at the shoulder joint, which has a complex structure (as detailed in Section II).

This work supported by NSF EFRI Grant #1137267

Authors affiliated with Department of Mechanical Engineering, University of California, Berkeley, CA 94720 USA (e-mail: {khaninger, junkai.lu, wjchen, tomizuka}@berkeley.edu)

This paper first presents a motion capture algorithm to find the center of a joint from motion capture data. This algorithm is extended to study the motion of the shoulder joint, validated with human data, then used to develop a model of the macaque sholder complex. These results are incorporated in a design which uses a mechanically coupled degree of freedom (DOF) to improve joint alignment at the shoulder complex. A kinematic analysis of this design is introduced to determine maximum joint speeds required in the workspace.

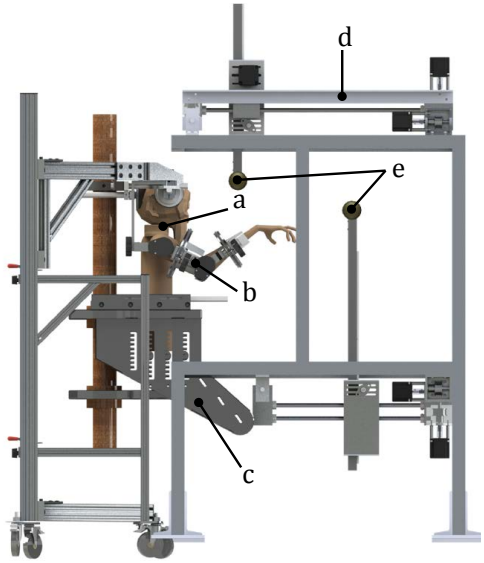

Fig. 1. Overview of project hardware (a. Macaque subject, b. Upper-limb exoskeleton, c. Primate chair, d. Target presentation system, e. Interactive targets)

II. SHOULDER COMPLEX

A. Human Shoulder Complex

The various objectives for the exoskeleton require the ability to safely apply torques to a subject and accurately measure joint angles. To achieve the safe transmission of torque and accurate measurement of joint angles, the mechanical revolute joint axis must be aligned with the biological joint axis. Misalignment introduces undesired internal forces in the subject, as the exoskeleton attachment point follows a different path than that naturally followed by the subject. Additionally, if the axes are misaligned, the joint angle of the exoskeleton will not match that of the subject.

Though joint alignment is critical for the objectives of an exoskeleton, it is complicated by the irregular nature

of biological joints. Biological joints result from contact between two irregular bony surfaces, and thus the axis of rotation may change with the joint angle. Joints such as the elbow are well modelled by a revolute joint [1], however, more complex joints present more challenges. For example, the human shoulder joint is commonly considered a 'ball-and-socket' joint, with three rotational DOFs. However, the glenohumeral (GH) joint (the ball-and-socket joint) is not rigidly fixed relative to the torso, but is a member of a kinematic chain which connects the torso to the humerus, as seen in Fig. 2. Thus, the GH joint can translate, subject to the constraints of the supporting bones, joints and ligaments. While a complete model of the shoulder would characterize all the supporting bones, a simplified model which captures the majority of the shoulder behavior is a 5 DOF model, as proposed by [2]. The three rotational DOFs are about the shoulder center of rotation (CoR), which roughly coincides with the center of the GH joint [1]. An additional two DOFs are the translation of the shoulder CoR in elevation/depression and protraction/retraction. These translational DOFs can be actuated to some degree independently of arm posture, but nominal relationships between humerus posture and translation of the shoulder CoR in humans have been proposed in [1], [3].

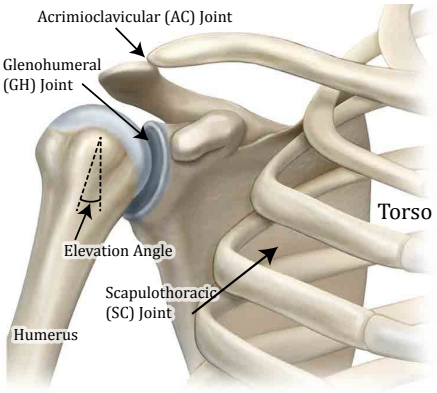

Fig. 2. Human right shoulder, front view [4]

Matching a high DOF shoulder model in an exoskeleton is difficult, and the complexity required to have 3 passive translational DOFs at the shoulder (as in [5]) would risk making this exoskeleton fragile to a non-compliant subject. Other designs propose alternatives to the revolute joint, such as [6], which introduces two passive translational DOFs at a revolute joint. In general, these passive translational DOFs remove the ability to precisely position the end effector, which is problematic for the reaching and grasping task this exoskeleton is designed for.

Other designs have simplified model of the shoulder which captures the dominant translation, and established a fixed relationship between some of the DOFs so the mechanism is fully determined by the actuated joints. ARMIN II [7] and ARMIN III [3] introduce a mechanically coupled passive DOF. These mechanisms raises the shoulder CoR as the arm is elevated, approximately following the vertical shoulder CoR translation. The linkages which drive this relationship can be adjusted, but arbitrary translation relationships cannot be realized. Most common is to allow only three rotational DOF at the shoulder complex [8], [9], [10]. Though mechanically simpler, this stationary CoR may limit the comfortable range of motion [11].

Even in humans, where shoulder behavior has been well-studied, a variety of models for the shoulder have been incorporated in exoskeleton designs. As the macaque physiology is similar, but of different dimensions from humans [12], the shoulder CoR may translate more dramatically in different directions for macaques. To justify an ergonomic design, the shoulder center behavior must be known for macaques.

B. Shoulder Center Analysis

Motion capture systems allow new means of studying kinematics by recording the 3D position of a collection of markers. Under some assumptions about the markers (e.g. rigidly attached), the motion of the markers can be used to determine characteristics of the underlying structure to which they are fixed. For example, motion capture techniques have been used to locate the center of the hip joint, well modelled as a non-translating ball-and-socket joint. Some algorithms assume the markers stay a fixed distance from the CoR [13], [14]. Other algorithms assume that these markers are fixed to a body which undergoes a rigid body transformation (a translation and rotation which preserves distances between points) [15]. While these algorithms have been successful with humans, they estimate the hip center as a fixed CoR, while here it is desired to know how the shoulder CoR translates.

To characterize the shoulder CoR translation over different humerus postures, it is assumed that the shoulder CoR location is strictly a function of humerus orientation [1]. The data is then seperated into bins which divide the task space according to the orientation of the humerus. For appropriately small bins, it is then assumed that the shoulder CoR is stationary inside each of these bins. To find the shoulder CoR inside each bin, the following algorithm is proposed, which operates on data collected from at least 3 markers affixed to the torso, and at least three markers affixed to the upper arm (three or more markers allow calculation of rigid body transformations).

1) Torso markers are used to normalize the data. A least squares (LS) rigid body transformation [16] is found between the first frame and each subsequent frame, and the inverse of each frame's transformation applied to hold the torso markers roughly fixed. Reducing the recorded translation of the torso prevents that motion from being attributed to the motion of the shoulder CoR.
2) Within each bin, K pairs of frames are randomly chosen, and rejected if the change in humerus pose is below a threshold.
3) For each pair of frames, an equivalent axis of rotation is found (see below for details).

4) An initial appoximation for the CoR in the bin is found by a LS technique [14] and used to remove outlying axes.
5) The remaining axes will, for real-world data, be skew. The point which minimizes distance to all remaining axes is found, and taken as the CoR.

Between two frames of 3D data, an axis of rotation which relates the two frames is estimated. For a rigid body with a fixed point (the CoR is assumed to be fixed for data within a bin), any rigid body transformation can be expressed strictly as a rotation about an axis through that point [17]. Two collections of M markers, $X_i := \left[x_i^1, x_i^2, \ldots, x_i^M\right] \in \mathbb{R}^{3\times M}$ and X_j (similarly defined) represent the position of M markers at times i and j respectively. The centroid over all the markers at the two times, c_i and c_j are found, and a rotation matrix $R^{i\to j}$ found to minimize:

$$\sum_{k=1}^{M} \| \left(x_j^k - c_j\right) - R^{i\to j}\left(x_i^k - c_i\right) \|_2^2 \qquad (1)$$

As detailed in [16], the optimal solution can be found given the singular value decomposition (SVD) of $\sum_{k=1}^{M}(x_j^k - c_j)(x_i^k - c_i)^T = USV^T$ as $R^{i\to j} = UV^T$. The translation can be found as $t^{i\to j} = c_j - R^{i\to j}c_i$. The rotation matrix $R^{i\to j}$ can be converted to an axis-angle representation $\left(v^{i\to j}, \theta^{i\to j}\right)$, where $v^{i\to j}$ is the equivalent axis of rotation and $\theta^{i\to j}$ denotes the amount of rotation about that axis [18].

The axis-angle represntation of the rotation gives only the orientation of the axis, not its position in 3D space. The rotation axis will be normal to a plane which contains the translation $t^{i\to j}$, and will be equidistant from both the centroids, as illustrated in Fig. 3. This defines an isoceles triangle in the plane normal to the rotation axis, where $(\theta^{i\to j},\ t^{i\to j})$ are sufficient to solve for the position of the axis. This axis can then be added to the collection of axes which is used to estimate the CoR.

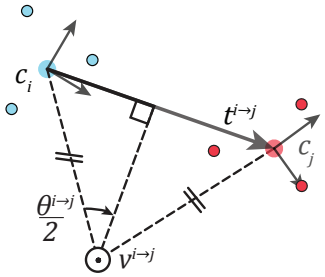

Fig. 3. Localizing the axis of rotation

This algorithm has several components specifically introduced to address the noise in motion capture data. In addition to expected noise from camera observations, camera switching errors and other sources can result in some axis estimates diverging from the other estimates. These outliers are removed in the algorithm. Also, only large changes in pose are compared, because for smaller motions the noise dominates the rigid body transformations and gives inconsistent results.

C. Results

The algorithm was first applied to data from a human subject (male, 23 years old, 189 cm), to validate the algorithm with comparison to accepted results for human shoulder center motion. The results in literature were obtained using other (not motion capture based) techniques. [3] uses a model of the geometry of the clavicle, scapula, and rib cage, along with estimates of their poses, to generate a forward kinematics estimate for the translation of the shoulder CoR. In [1], x-ray photographs were taken of subjects as the arm was elevated in 15° increments, and the shoulder center taken as the center of the humerus head. To compare with these results, the human collected data was binned on arm elevation angle (the angle between the humerus and the torso, as illustrated in Fig. 2), plotted with numbers corresponding to increasing arm elevation angle ranges (e.g. Bin 1 for 0-15deg, Bin 2 for 15-30deg,...). Shown in Fig. 4, the overall range corresponds with the established results, and the form of the path the shoulder travels is also similar. Shown for reference in Fig. 4 is the motion of a marker proximal to the acrimioclavicular (AC) joint of the subject, which is near the shoulder CoR but does not exactly match its translation due to motion of the underlying muscle mass.

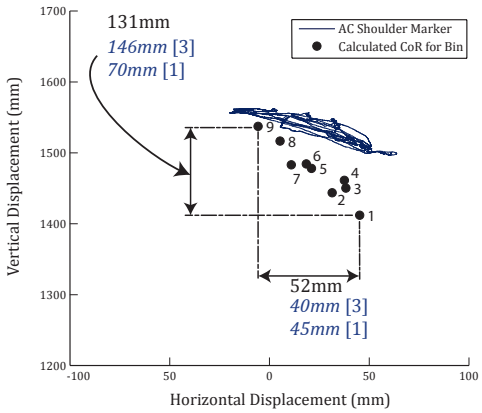

Fig. 4. Computed right human shoulder CoR, posterior view comparison

Following this validation, data was collected from a macaque subject (male, 7 years old, 10.5 kg). All procedures were conducted in compliance with the National Institute of Health Guide for Care and Use of Laboratory Animals and were approved by the University of California, Berkeley Institutional Animal Care and Use Committee. Markers were affixed to a tailored spandex shirt, with 5 markers on the torso and 7 on the upper right arm. The sedated subject wearing the shirt is then placed in the workspace of a PhaseSpace Improv system [19], and the subject's arm manually moved through the range of motion. It is assumed that the sedation and ensuing relaxation of voluntary muscles does not largely impact the behavior of the shoulder CoR.

To determine in what direction the macaque's shoulder CoR translation was most significant, the data was split by the position of a marker on the elbow into bins which evenly divided the 3D workspace. The results, seen in Table

I suggest that the elevation/depression of the shoulder CoR is the most significant translation of the shoulder CoR. As the elevation angle of the arm is most strongly linked with elevation/depression of the CoR [1], further studies were performed binning the data according to arm elevation angle.

TABLE I
RANGE OF MACAQUE SHOULDER COR MOTION

Direction	CoR range (mm)	AC Marker Range (mm)
Cranial (elevation)	53	49
Ventral (abduction)	37	26
Lateral	34	41

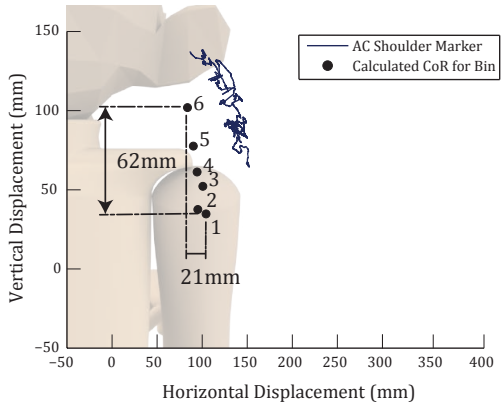

Fig. 5. Computed right macaque shoulder CoR

Fig. 5 shows the translation of the macaque shoulder CoR in the coronal plane when binned on arm elevation angle. The vertical motion of the shoulder CoR is detailed in Table II.

TABLE II
ELEVATION OF SHOULDER CENTER

Humerus Elevation (deg)	CoR Vertical Motion (mm)
0-20	0
20-40	4
40-60	13
60-80	27
80-100	43
100-120	62

III. KINEMATIC DESIGN

This relationship between arm elevation angle and shoulder center position was then used in a design which uses a cam to raise the center of the exoskeleton shoulder as the arm is elevated. Only the vertical translation of the shoulder center is matched in this design. The vertical translation has the widest range, and is the most difficult to compensate by a seated subject. Shoulder motion in the transverse plane (lateral movement) can be compensated by torso movement of the subject, while vertical shoulder motion cannot be easily achieved by a subject who remains seated.

The shoulder cam design is detailed in Fig. 6, where the cam rotates as the arm is raised, and pushes on a fixed support to elevate the mechanism along slide rails. The profile of the cam is designed so that at a given angle of elevation, the center has been raised by the amount determined in the motion capture study. The 6 elevation points and the angles at which they occur were used to define a spline which smoothly connects them.

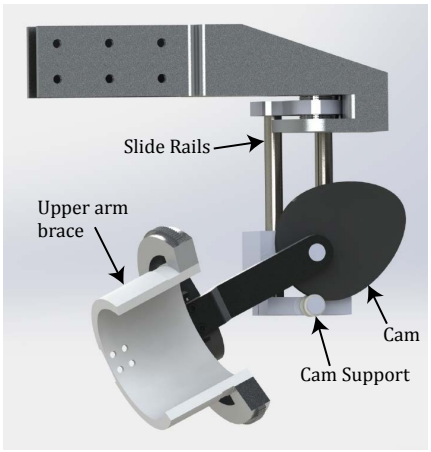

Fig. 6. Detail of shoulder cam mechanism

The complete design, shown in Fig. 7 features 5 powered DOFs, with 3 DOFs at the shoulder, and a mechanically coupled DOF to allow the vertical motion of the shoulder complex. An additional DOF is placed at the elbow, and another to allow pronation/supination of the wrist. The 3 most distal DOF (internal/external rotation of the arm, elbow, pro/supination) are driven by a Bowden cable driven system to reduce the inertia of the mechanism. Following the concept of a series-elastic actuator [20], the joints have introduced compliance through a spring, which ensures safety of the subject by decoupling the actuator angle and the subject angle, as well as allowing measurement of applied torque by measuring the relative deflection of the spring.

IV. KINEMATIC ANALYSIS

Serial revolute joints are often used in robotic devices due to the ease with which a revolute joint can be implemented and actuated. However, one issue faced by serial revolute mechanisms is the alignment of joint axes from two or more DOFs. Parallel axes can no longer affect motion in independent directions, and may reduce the ability of the end effector to realize certain rotational or linear velocities. If there is an instantaneous loss of ability to realize end effector motion at a given pose, it is termed a kinematic singularity. In the proposed exoskeleton, a three DOF shoulder joint is realized with three serial revolute joints, and the alignment of the first and third axes is possible, which results in a singularity. To preserve the ability to realize arbitrary motion, other researchers have introduced additional DOF [21] or placed the singularity outside the expected joint workspace [11]. For this mechanism, the singularity occurs at the home position

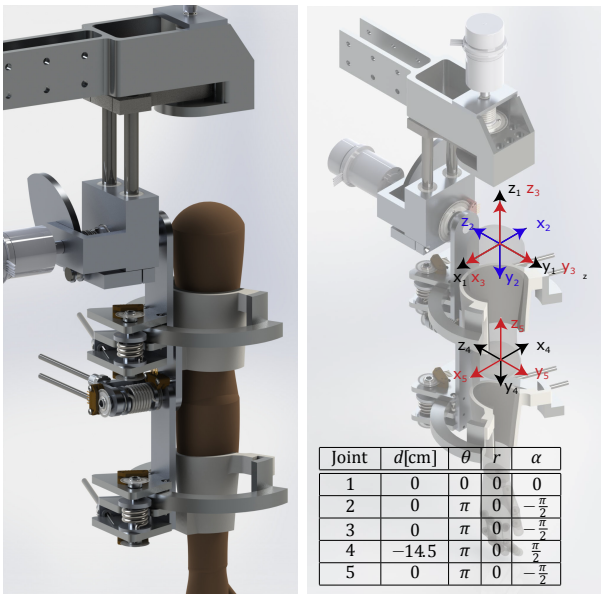

Joint	d[cm]	θ	r	α
1	0	0	0	0
2	0	π	0	$-\frac{\pi}{2}$
3	0	π	0	$-\frac{\pi}{2}$
4	−14.5	π	0	$\frac{\pi}{2}$
5	0	π	0	$-\frac{\pi}{2}$

Fig. 7. Exoskeleton in the home posture (with standard DH parameters)

shown in Fig. 7. This posture places the end effector outside of the task workspace, and so the complexity associated with additional DOF or singularity placement have been omitted. However, the kinematic behavior of the exoskeleton may deteriorate in the neighborhood of the singularity, which may be within the workspace.

A. Manipulability

Manipulability is a measure used to compare how close different designs are to a singular configuration. Assume a configuration is described by joint angles $\theta \in \mathbb{R}^J$, end effector motion $\dot{x}_{ee} \in \mathbb{R}^N$ (translational, rotational, or both) and a Jacobian $J(\theta) : \mathbb{R}^J \rightarrow \mathbb{R}^N$ which maps the joint speeds to end effector motion as $\dot{x}_{ee} = J(\theta)\dot{\theta}$. The manipulability as proposed by [22] is:

$$w(\theta) = \sqrt{\det\left(J(\theta) J^T(\theta)\right)} \tag{2}$$

The same arguments hold for relative manipulability, proposed in [23], which normalizes for link dimensions, dimension order of task space, and number of DOF. Taking the SVD, the manipulability can be expessed in another way:

$$\sqrt{\det\left(JJ^T\right)} \quad = \quad \prod_{i=1}^{N} \sigma_i \tag{3}$$

where σ_i is the i^{th} singular value, and N is the dimension of desired velocities (e.g. 6 for linear and rotational velocities in a 3D task space). If a pose θ_s gives a manipulability $w(\theta_s) = 0$, θ_s is a singular pose. As a singular value σ_i approaches zero, achieving velocities in the task space along the corresponding direction requires large joint velocities.

Manipulability can be used to compare proximity to singularity between designs, but it may not distinguish between the required joint velocities. If the product of singular values are the same, the manipulability is the same, regardless of the Jacobian's condition number (the ratio of largest and smallest singular values). However, a smaller singular value means end effector velocities in the degenerated direction require larger joint velocities. Though two designs in a pose may have comparable manipulability, if they have different condition numbers, they may require different joint speeds for similar end effector motion. As larger joint velocities are difficult to achieve with physical actuators, the maximum joint speed may be of interest as a relative value to compare between designs, or as an absolute value for selecting the gearbox on an actuator.

B. Maximum Joint Speed

The following analysis finds bounds on required joint speed to realize a known end effector speed $v_{max} \in \mathbb{R}$ across all poses within the workspace. This analysis only examines translational end effector speed, though similar analysis could be performed for a desired end effector rotational speed.

1) Non-redundant Manipulators: Given a (non-singular) pose θ, the joint speeds that are needed to achieve v_{max} in an arbitrary direction can be found in:

$$\begin{aligned} J(\theta)\dot{\theta} &= v_{max} \cdot u, \qquad \forall \|u\|_2 = 1 \\ \Rightarrow \dot{\theta}^T J^T(\theta) J(\theta) \dot{\theta} &= v_{max}^2 \end{aligned} \tag{4}$$

where u is a unit vector to represent that v_{max} can be in an arbitrary direction. The last equality in (4) defines an ellipsoid, as in this posture, J is full rank, making $J^T J$ positive definite. The maximum speed for joint i can then be found as the maximum $\dot{\theta}_i$ such that $(\dot{\theta}_1, .., \dot{\theta}_i, .., \dot{\theta}_M)$ satisfy (4).

2) Extension to Redundant Manipulators: A redundant manipulator, such as the 5DOF mechanism proposed here (when only considering linear workspace velocities) has a Jacobian with a non-empty nullspace, implying $J^T J$ is positive semi-definite and thus (4) does not define an ellipsoid. Arbitarily large joint velocities from the nullspace of J can be added to $\dot{\theta}$ while (4) holds true. This is not informative to determine an upper bound to the joint velocities.

One way to extend the analysis to redundant manipulators is to look at the most common form of inverse kinematics. The pseudo-inverse of the Jacobian is typically used to determine the joint velocities from a desired end effector velocity. Using the pseudo-invese gives a minimum 2-norm solution to the equation $v = J\dot{\theta}$, a $\dot{\theta}$ which has no component in the nullspace of J. If this nullspace avoidance is added as a constraint to (4), then the maximum joint velocities required can be found if the inverse kinematics are done via the pseudoinverse.

3) Analysis of Proposed Exoskeleton: Over the workspace for the exoskeleton, as defined by the target positioning system in Fig. 1, the maximum joint angle speeds were calculated for the first four joints. The 5th joint has no contribution to the linear velocity of the end effector in the workspace. The desired end effector speed was found from motion capture data. A marker was affixed to the wrist of the (awake) Macaque subject, and the subject reached for a

treat arbitrarily positioned, a task similar to the final experimental task for which the exoskeleton is being designed. The maximum speed achieved in this reaching task was then set as the v_{max} in the algorithm outlined above. The Robotics Toolbox [24] was then used to generate Jacobians (with the DH parameters in Fig. 7) by discretizing over the θ range of motion, and keeping those poses which placed the end effector within the workspace. Then, for each pose which places the end effector in the workspace, an optimization toolbox, CVX [25], was used to solve the optimization problem in (5). At each pose, this optimization problem was run for each joint, to find the maximum $\left|\dot{\theta}_i\right|$. Finally, the maximum speed for each joint i is taken over all poses in the workspace to find the bounds shown in Table III.

$$\max_{\dot{\theta}} |\dot{\theta}_i| \quad \text{s.t.} \quad \dot{\theta}^T J(\theta)^T J(\theta) \dot{\theta} = v_{max}^2 \qquad (5)$$
$$\dot{\theta} \perp \text{Null}(J(\theta))$$

TABLE III
BOUNDS ON JOINT VELOCITIES TO ACHIEVE v_{max}

Joint	Max Speed (rad/sec)
1: Shoulder Ab/adduction	.64
2: Shoulder Flexion/extension	1.06
3: Shoulder Internal/External Rotation	1.80
4: Elbow Flexion/Extension	5.38

V. CONCLUSION

This paper presented new techniques for the design and analysis of an exoskeleton with an emphasis on maintaining joint alignment at the shoulder. Improving joint alignment is key to exoskeleton performance, and maintaining the comfort of the subject. A novel algorithm for determing the center of rotation was presented, and validated on human data. This algorithm was then applied to data collected from one of the macaques subjects, and the results of this study used to motivate an exoskeleton which matches the dominant motion of the shoulder center in macaques.

A complement to the manipulability measure was introduced, which determines an upper limit on joint speeds which are required to realize a given end effector speed arbitrarily in the workspace. The proposed kinematic analysis gives results which have immediate physical interpretations, and can be useful in actuator design.

ACKNOWLEDGMENT

We would like to thank Dr. Simon Overduin and Suraj Gowda for help with data collection.

REFERENCES

[1] Z. Dvir and N. Berme, "The shoulder complex in elevation of the arm: a mechanism approach," *J. of Biomechanics*, vol. 11, no. 5, pp. 219–225, 1978.

[2] J. Yang, K. Abdel-Malek, and K. Nebel, "Reach envelope of a 9-degree-of freedom model of the upper extremity," *Int. J. of Robotics and Automation*, vol. 20, no. 4, pp. 240–259, 2005.

[3] T. Nef, M. Guidali, and R. Riener, "ARMin III–arm therapy exoskeleton with an ergonomic shoulder actuation," *Applied Bionics and Biomechanics*, vol. 6, no. 2, pp. 127–142, 2009.

[4] Image used courtesy of Ion Medical Designs http://ionmedicaldesigns.com.

[5] F. Martinez, I. Retolaza, A. Pujana-Arrese, A. Cenitagoya, J. Basurko, and J. Landaluze, "Design of a five actuated DoF upper limb exoskeleton oriented to workplace help," in *Biomedical Robotics and Biomechatronics (BioRob), 2008. 2nd IEEE RAS & EMBS Int. Conf. on*, pp. 169–174.

[6] M. A. Ergin and V. Patoglu, "ASSISTON-SE: A self-aligning shoulder-elbow exoskeleton," in *Robotics and Automation (ICRA), 2012 IEEE Int. Conf. on*, pp. 2479–2485.

[7] M. Mihelj, T. Nef, and R. Riener, "ARMin II-7 DoF rehabilitation robot: mechanics and kinematics," in *Robotics and Automation (ICRA), 2007 IEEE International Conference on*, pp. 4120–4125.

[8] J. C. Perry, J. Rosen, and S. Burns, "Upper-limb powered exoskeleton design," *Mechatron, IEEE/ASME Trans. on*, vol. 12, no. 4, pp. 408–417.

[9] G. Johnson, D. Carus, G. Parrini, S. Marchese, and R. Valeggi, "The design of a five-degree-of-freedom powered orthosis for the upper limb," *Proc. of the Institution of Mechanical Engineers, Part H: J. of Eng. in Medicine*, vol. 215, no. 3, pp. 275–284, 2001.

[10] P. Letier, M. Avraam, S. Veillerette, M. Horodinca, M. De Bartolomei, A. Schiele, and A. Preumont, "SAM: A 7-DOF portable arm exoskeleton with local joint control," in *Intelligent Robots and Systems (IROS), 2008. IEEE/RSJ Int. Conf. on*, pp. 3501–3506.

[11] S. J. Ball, I. E. Brown, and S. H. Scott, "MEDARM: a rehabilitation robot with 5DOF at the shoulder complex," in *Advanced Intelligent Mechatronics (AIM), 2007 IEEE/ASME Int. Conf. on*, pp. 1–6.

[12] E. J. Cheng, S. H. Scott *et al.*, "Morphometry of Macaca mulatta forelimb," *J. of Morphology*, vol. 245, no. 3, pp. 206–224, 2000.

[13] V. Camomilla, A. Cereatti, G. Vannozzi, and A. Cappozzo, "An optimized protocol for hip joint centre determination using the functional method," *J. of Biomechanics*, vol. 39, no. 6, pp. 1096–1106, 2006.

[14] L. Y. Chang and N. S. Pollard, "Constrained least-squares optimization for robust estimation of center of rotation," *J. of Biomechanics*, vol. 40, no. 6, pp. 1392–1400, 2007.

[15] M. H. Schwartz and A. Rozumalski, "A new method for estimating joint parameters from motion data," *J. of Biomechanics*, vol. 38, no. 1, pp. 107–116, 2005.

[16] S. Umeyama, "Least-squares estimation of transformation parameters between two point patterns," *Pattern Anal. Mach. Intell., IEEE Trans. on*, vol. 13, no. 4, pp. 376–380, 1991.

[17] H. Cheng and K. Gupta, "An historical note on finite rotations," *ASME Trans. Series E J. of Applied Mechanics*, vol. 56, pp. 139–145, 1989.

[18] B. Siciliano and O. Khatib, *Springer handbook of robotics*. Springer, 2008.

[19] PhaseSpace Inc. The IMPULSE X2 Motion Capture System Catalog. [Online]. Available: http://www.phasespace.com/products/ImpulseProductDoc.pdf.

[20] K. Kong, J. Bae, and M. Tomizuka, "Control of rotary series elastic actuator for ideal force-mode actuation in human–robot interaction applications," *Mechatron., IEEE/ASME Trans. on*, vol. 14, no. 1, pp. 105–118, 2009.

[21] J. Lu, W. Chen, and M. Tomizuka, "Kinematic Design and Analysis of a 6-DOF Upper Limb Exoskeleton Model for a Brain-Machine Interface Study," in *Proc. 6th IFAC Symp. on Mechatronic Syst.*, 2013, pp. 293–300.

[22] T. Yoshikawa, "Manipulability of robotic mechanisms," *The Int. J. of Robotics Research*, vol. 4, no. 2, pp. 3–9, 1985.

[23] J.-O. Kim and P. K. Khosla, "Dexterity measures for design and control of manipulators," in *Intelligent Robots and Systems (IROS), 1991. IEEE/RSJ Int. Conf. on*. IEEE, 1991, pp. 758–763.

[24] P. I. Corke, *Robotics, Vision & Control: Fundamental Algorithms in Matlab*. Springer, 2011.

[25] M. Grant and S. Boyd, "CVX: Matlab software for disciplined convex programming, version 2.0 beta," http://cvxr.com/cvx, Sep. 2013.